Metallophysics and Advanced Technologies
Металофіз. новітні технол.
Metallofiz. Noveishie Tekhnol.
2025, vol. 47, No. 7, pp. 675–701
https://doi.org/10.15407/mfint.47.07.0675
Reprints available directly from the publisher

PACS numbers: 07.05.Tp, 75.50.Bb, 75.50.Tt, 84.30.Bv, 84.30.Vn, 84.32.Hh, 85.70.Ay

Modelling of DC-Bias Stable Chokes Based on Nanocrystalline $Fe_{73}Si_{16}B_7Cu_1Nb_3$ Cores

B. S. Baitaliuk, V. K. Nosenko, O. V. Oliinyk, O. M. Semyrga

G. V. Kurdyumov Institute for Metal Physics, N.A.S. of Ukraine,
36 Academician Vernadsky Blvd.,
UA-03142 Kyiv, Ukraine

The application of the nanocrystalline $Fe_{73}Si_{16}B_7Cu_1Nb_3$ alloy for the fabrication of toroidal-core inductors (chokes) operating under DC-bias conditions is investigated. The influence of the $Fe_{73}Si_{16}B_7Cu_1Nb_3$-alloy properties, particularly, its high magnetic permeability and thermal stability of magnetic properties, on the choke characteristics is studied. A novel calculation method for the dimensions and number of turns of toroidal chokes, considering specified parameters and operating modes, is proposed. This method incorporates the analytical and numerical techniques to determine the optimal core dimensions and number of wire turns, ensuring minimal losses and high choke efficiency. This efficiency manifests itself in reduced energy losses, improved size and weight characteristics, enhanced manufacturability, and ensuring stable choke operation under various operating modes. A software algorithm for automated calculation of choke parameters is developed, enabling rapid and accurate calculations, considering all key parameters such as inductance, operating flux density, and wire cross-section. An analysis of the influence of the number of wire turns and the magnetic permeability of the $Fe_{73}Si_{16}B_7Cu_1Nb_3$ alloy on the geometrical dimensions, weight, and electromagnetic losses of the chokes is performed. The proposed method allows for optimizing the choke design, reducing their weight and cost that is crucial for industrial applications, especially, in areas, where compact and efficient inductive components with low losses are required.

Corresponding author: Bohdan Serhiyovych Baitaliuk
E-mail: baytalyuk@ukr.net

Citation: B. S. Baitaliuk, V. K. Nosenko, O. V. Oliinyk, and O. M. Semyrga, Modelling of DC-Bias Stable Chokes Based on Nanocrystalline $Fe_{73}Si_{16}B_7Cu_1Nb_3$ Cores, *Metallofiz. Noveishie Tekhnol.*, **47**, No. 7: 675–701 (2025), DOI: 10.15407/mfint.47.07.0675

Key words: nanocrystalline alloy, inductors/chokes, DC bias, magnetic permeability, toroidal core.

Досліджено застосування нанокристалічного стопу $Fe_{73}Si_{16}B_7Cu_1Nb_3$ для виготовлення котушок індуктивности (дроселів) з тороїдальним магнетопроводом, що працюють в умовах підмагнетування постійним струмом. Вивчено вплив властивостей стопу $Fe_{73}Si_{16}B_7Cu_1Nb_3$, зокрема його високої магнетної проникности та термічної стабільности магнетних властивостей, на характеристики дроселів. Запропоновано нову методику розрахунку габаритів і кількости витків тороїдальних дроселів, яка враховує задані параметри та робочі режими. Ця методика включає аналітичні та чисельні методи для визначення оптимальних розмірів осердя та кількости витків проводу, забезпечуючи мінімальні втрати та високу ефективність дроселів, яка полягає у пониженні енергетичних втрат, поліпшенні масогабаритних характеристик, підвищенні технологічности виробництва та забезпеченні стабільности роботи дроселів під час різних робочих режимів. Розроблено програмний алґоритм для автоматизованого розрахунку параметрів дроселів, що дає змогу швидко та точно проводити розрахунки, враховуючи всі ключові параметри, такі як індуктивність, робоча індукція та переріз проводу. Проведено аналізу впливу кількости витків проводу та магнетної проникности стопу $Fe_{73}Si_{16}B_7Cu_1Nb_3$ на геометричні розміри, масу й електромагнетні втрати дроселів. Запропонований метод уможливлює оптимізувати конструкцію дроселів, зменшити їхню вагу та вартість, що є критично важливим для промислового застосування, особливо у сферах, де потрібні компактні й ефективні індуктивні компоненти з низькими втратами.

Ключові слова: нанокристалічний стоп, котушка індуктивности, дросель, підмагнетування, магнетна проникність, тороїдальне осердя, магнетопровід.

(Received 16 January, 2025; in final version, 7 April, 2025)

1. INTRODUCTION

Modern electronic and electrical devices cannot function without inductive components such as chokes, filters, transformers, and sensors [1–9]. Considering current trends towards miniaturization and high efficiency in electronics and microelectronics, the magnetic cores for these components are predominantly made of magnetodielectrics.

Along with traditional materials for magnetodielectric production, which have been actively used for a long time (composites based on iron powders, AlSiFe, permalloys, Fe–Si system alloys and their mixtures) [10–18], composites based on amorphous and nanocrystalline alloy powders are becoming increasingly widespread [19–24]. Amorphous alloys, due to their unique properties, such as high electrical resistivity and low eddy-current losses, are ideal for the production of inductive components operating in high-frequency modes [25–28].

Nanocrystalline alloys are particularly promising due to their exceptional soft magnetic properties, including high magnetic permeability, low core losses (losses on remagnetisation), and high saturation induction [29–32]. One such alloy is $Fe_{73}Si_{16}B_7Cu_1Nb_3$ (of the 'FINEMET' type [33]), which is obtained by special heat treatment of the initial amorphous ribbon [34, 35]. This alloy exhibits high magnetic permeability, low core losses, and temperature stability of magnetic properties [36–40], making it an ideal material for inductive components operating under DC bias conditions.

For effective ripple smoothing at the output of a rectifier in switching power supplies, chokes with high AC resistance and low DC resistance are used. Chokes using the $Fe_{73}Si_{16}B_7Cu_1Nb_3$ alloy have significant potential for application in various promising fields. In particular, they can be used in electric vehicles for effective electric motor control and reduction of electromagnetic interference. In renewable energy, such chokes can be integrated into energy conversion systems, such as wind and solar inverters, where high stability and low losses are critical. They can also find application in telecommunication systems for signal stabilization and equipment protection from interference. The inductance stability of a linear choke throughout the entire operating range of the direct current passing through its winding is a key requirement, which can be easily achieved using nanocrystalline alloys, allowing the creation of compact and efficient inductive components that meet the high demands of modern technologies.

At the current stage of development in electronics and electrical engineering, numerous works on the calculation methods for transformers and chokes in various operating modes have emerged. Thus, the authors [8, 41, 42] present a calculation method for so-called shell-type and core-type coils, but pay little attention to toroidal chokes. The formulas and calculation methods they use rely on correction factors and graphical-analytical calculation methods. Furthermore, the lack of powerful computing complexes at that time did not allow the authors to perform computer simulations to solve the problems. The authors calculate inductance depending on voltage, current, and frequency, and also pay attention to the quality factor of inductors and losses in the core and wire material.

In studies [43, 44], the dimensions of the magnetic core are assessed differently for transformers and inductors (chokes). For a transformer, this is $S_c \times S_o$—the product of the core cross-sectional area (S_c) and the window area with the winding (S_o), while, for an inductor, it is the core volume $S_c \times l_c$—the product of the core cross-sectional area and the mean magnetic path length (l_c). This approach complicates the comparative assessment of the dimensions of different electromagnetic components.

In study [45], a method for calculating the inductor for a Class-E power amplifier with zero-voltage switching (ZVS) is proposed. The methodology encompasses the design of the inductor inductance and a theoretical assessment of power losses. The authors employed the Area-Product (A_p) method for inductor design and a calculation algorithm comprising the following steps.

1) Determining the maximum energy, which the inductor can store:

$$W_{\mathrm{Lf}} = \frac{1}{2} L_{\mathrm{f}} I^2_{\mathrm{Lf(max)}},$$

where L_f is the specified inductance, and $I_{\mathrm{Lf(max)}}$ is the peak value of the operating current.

2) Determining the core area product, which is defined as the product of the core cross-sectional area (core area) and the window area, through which the winding passes:

$$A_{\mathrm{p}} = W_{\mathrm{a}} A_{\mathrm{c}} = \frac{4W_{\mathrm{Lf}}}{K_{\mathrm{u}} J_{\mathrm{m}} B_{\mathrm{sat}}},$$

where W_a is the window area of the core, A_c is the cross-sectional area, K_u is the fill factor of the wire, W_{Lf} is the energy stored by the inductor, J_m is the current density flowing through the inductor winding, and B_s is the saturation flux density of the core material.

3) Determining the number of turns of the wire:

$$N = \max\left\{\frac{W_{\mathrm{a}} K_{\mathrm{u}}}{2A_{\mathrm{w(sol)}}}, \sqrt{\frac{L_{\mathrm{f}}}{\mu_0 A_{\mathrm{c}}}\left(l_{\mathrm{g}} + \frac{l_{\mathrm{c}}}{\mu_{\mathrm{rc}}}\right)}\right\},$$

where μ_0 is the permeability of free space, μ_{rc} is the relative permeability of the core material, N is the number of turns of the wire, l_g is the mean length of the magnetic flux path, l_c is the effective length of the air gap, and $A_{\mathrm{w(sol)}}$ is the cross-sectional area of one turn of the wire.

4) Determining the operating flux density of the inductor:

$$B_{\mathrm{pk}} = \frac{\mu_{\mathrm{rc}} \mu_0 N I_{\mathrm{Lf(max)}}}{l_{\mathrm{c}}\left(1 + \frac{\mu_{\mathrm{rc}} l_{\mathrm{g}}}{l_{\mathrm{c}}}\right)}.$$

5) Determining the losses, which include hysteresis losses, core losses, and winding losses:

$$P_{\mathrm{tot}} = P_{\mathrm{c}} + P_{\mathrm{w}} + P_{\mathrm{wac}}.$$

While this approach allows for the efficient calculation of the number of turns, operating flux density, and accurate estimation of power losses, it has certain drawbacks. In particular, this method does not provide a precise calculation of the inductor geometry, as the geometry is determined based on catalogues according to the calculated product area values. Furthermore, the calculation of the number of turns is ambiguous, as one value is chosen based on the results of calculations using two separate formulas. The inductor calculation methodology does not consider all necessary parameters, and each value is calculated separately, which requires the use of successive iterations. This complicates the automation of the process and leads to the necessity of using a trial-and-error method.

Paper [2] investigates the relationship between inductance and operating current of electromagnetic devices used in automotive systems. The authors conducted measurements of inductance and direct current for various automotive electromagnetic devices, such as relay coils, starter motors, fuel pumps, and others. The specificity of the described work lies in establishing a quantitative relationship that allows predicting the inductance of a device, knowing its operating current. The authors proposed an empirical formula to express this relationship:

$$L = \frac{8.62}{I^{1.3}},$$

where L is the inductance [mH], I is the current [A]. This formula was obtained through regression analysis of the measured data and demonstrates fairly accurate agreement with experimental results that allows it to be used for estimating the inductance of typical automotive electromagnetic devices.

The methodology proposed by the authors has several distinct advantages. First, it provides the ability to estimate quickly and accurately the inductance of automotive electromagnetic devices based on simple current measurements, which is crucial for practical applications, such as predicting spark formation in automotive electrical systems. Second, the proposed formula accurately describes general trends for a wide range of devices, including both low-power relays and high-power starters.

However, the methodology also has limitations. In particular, it exhibits some inaccuracy, especially, for devices with very low or very high inductance values, where deviations from the empirical formula are observed. The study also notes that the structure of the magnetic circuits of different devices can vary significantly, which can affect the accuracy of the predictions.

Overall, the study is of practical interest to the automotive industry, as it provides a simple and effective tool for estimating the inductance of electromagnetic devices based on their operating current, which can be beneficial in the context of designing and ensuring the safety of automotive electrical systems.

In William McLyman's book [46], two key parameters for transformer and inductor design are examined in detail: the geometry coefficient K_g and the area product A_p. These parameters are fundamental for the calculation and design of these devices. The K_g coefficient relates to the ability of the core to transfer effectively energy, while A_p characterizes the core volume required for transferring a specific power and is closely related to the current density in the windings.

Geometry Coefficient (K_g). The geometry coefficient K_g defines the relationship between the physical dimensions of the core and its ability to maintain a stable output power under varying loads. The K_g value considers both the core window area W_a and its cross-sectional area A_c, as well as the mean length per turn (MLT). The formula for determining the K_g coefficient is as follows:

$$K_g = \frac{W_a A_c^2 K_u}{MLT} [\mathrm{cm}^5],$$

where W_a is the core window area, A_c is the core cross-sectional area, K_u is the fill factor (or winding factor), and MLT is the mean length per turn of the wire.

This parameter allows designers to consider not only the core dimensions, but also its power handling capability based on its geometrical characteristics.

After determining the K_g value from calculations, a core from a catalogue that most closely matches this value must be selected. Since the exact K_g value for a specific core is not always available, the core selection process is often performed by trial and error. This means that the core dimensions, such as inner and outer diameter and height, cannot be calculated directly but are selected from standard options in the catalogue. This approach requires careful analysis and does not immediately yield optimal core dimensions, as it is limited by the available models in the catalogue.

Area Product (A_p). The area product A_p is another important parameter described by the author for calculating inductors operating under DC-bias conditions. It is defined as the product of the core window area W_a and the core cross-sectional area A_c:

$$A_p = W_a A_c = \frac{4W}{K_u J_m B_{sat}},$$

where K_u is the winding factor, W is the energy stored by the inductor, J_m is the current density flowing through the inductor winding, and B_s is the saturation flux density of the core material.

The A_p-based methodology is more straightforward but requires presetting the current density, which may lead to the need for additional iterations to achieve an optimal result. In addition, after calculating A_p, it is necessary to consult catalogues to select a core that matches the calculated parameters, which complicates the design process. Despite these drawbacks, the A_p-based approach allows for a quick assessment of the core dimensions and its compliance with power requirements.

The aim of this paper is to investigate the influence of geometrical dimensions (inner and outer diameters, height, cross-sectional area) and magnetic properties of cores made of nanocrystalline $Fe_{73}Si_{16}B_7Cu_1Nb_3$ alloy on the electrical losses (core losses) and efficiency of inductors. This alloy is characterized by high magnetic permeability, low hysteresis and eddy current losses, and high saturation flux density, making it promising for applications in inductive components. The proposed method for optimizing inductor design aims to reduce their weight and cost, which is crucial for industrial applications, especially in areas where compact and efficient inductive components with low losses and high stability are required (*e.g.*, switched-mode power supplies, electromagnetic interference filters, inverters). The main focus is on developing a new methodology for calculating the dimensions and number of turns of toroidal inductors, which takes into account specified parameters and operating modes.

An important aspect of the research is the influence of the magnetic permeability of magnetic cores based on the $Fe_{73}Si_{16}B_7Cu_1Nb_3$ alloy on the inductor characteristics, including their weight, dimensions, and electrical losses. Higher magnetic permeability allows achieving the required inductance with fewer turns, which leads to a reduction in winding losses and inductor size. The development of new calculation methodologies for such components will not only increase their efficiency and stability, but also reduce production costs. Thus, studying the application of nanocrystalline alloys for creating inductive components is relevant from a scientific and practical point of view, which allows solving a number of problems associated with reducing losses and increasing the operational stability of inductive components in electronic circuits, contributing to increased efficiency and reduced dimensions of electronic devices.

2. INDUCTOR DESIGN UNDER DC-BIAS CONDITIONS

2.1. Requirements for Inductors under DC-Bias Conditions

For effective ripple smoothing at the rectifier output in switching power supplies, inductors with high AC impedance and low DC resistance are used. These inductors are also used to protect the power line from impulse noise that can originate from the load. In switching power supplies operating on the principle of a forward converter, linear energy-storage inductors are used. They smooth DC current ripple by storing energy during current flow and maintaining current flow in the load circuit during off-times.

A key requirement is the inductance stability of a linear inductor over the entire operating current range flowing through its winding. This can be easily achieved by using cores made of nanocrystalline alloys with high saturation flux density.

For smoothing filters, which most often use such inductors, high-inductance inductors are required. Higher inductance provides greater AC impedance of the inductor, which allows reducing the size of the filter itself. Typically, such inductors are manufactured with cores made of ferromagnetic materials, such as iron, as well as various alloys, for example, permalloy, AlSiFe (Alfenol), Sendust [17].

However, the use of such cores causes a non-linear dependence of induction on field strength, as well as on the magnitude of the DC current flowing in the winding. The presence of a bias current reduces the magnetic permeability of the core and, consequently, the inductor performance. To mitigate this effect, a non-magnetic gap is introduced into the core material, using gapped or powdered cores (magnetic dielectrics).

With a non-magnetic gap, the magnetization curve becomes flatter, the core permeability decreases, and saturation occurs at significantly higher current values [8]. Both of these factors affect the inductor efficiency. Therefore, the task arises to calculate the optimal values of the core materials' magnetic permeability and the number of turns at given operating current values to obtain an inductor with minimal weight or cost.

2.2. Toroidal Core Inductor Design: Objectives and Methods

The design of toroidal inductors is a complex task requiring the consideration of numerous factors, such as core geometry, magnetic material properties, and operating conditions, including the effects of DC bias. Traditional design methods for these inductors are typically based on trial and error. Engineers select parameters through numerous experiments, which is not only time-consuming but also often leads to material waste and increased weight of the final product.

One of the main challenges is automating the design process of toroidal inductors. Existing calculation algorithms often do not account for all operating parameters and do not provide the necessary flexibility and accuracy, which complicates their use in a wide range of applications [47]. Weight optimization and material savings are also critical aspects, especially in modern manufacturing, where cost-effectiveness and maximum performance are key factors.

To solve these problems, it is necessary to develop a methodology that would allow calculations to be performed automatically with high accuracy. Such a methodology should consider all key parameters and their influence on the final inductance characteristics. This includes optimizing core geometry, selecting materials with the necessary magnetic properties, such as magnetic permeability, operating flux density, losses, and stability of magnetic properties over a wide temperature range. It is also necessary to consider the non-linear characteristics of the magnetic material at different bias current levels.

The proposed method of optimized design of inductors with toroidal gapped or powdered cores based on the $Fe_{73}Si_{16}B_7Cu_1Nb_3$ alloy allows automating this process and simplifying the calculation algorithm. Using specified parameters, such as required inductance, maximum current, and allowable bias current, the method allows automatically calculating the optimal dimensions and number of turns for the inductor. This ensures significant material savings and weight reduction of the product, which are important factors in many industrial applications.

The use of such a method avoids lengthy and costly experimental processes, reducing the development and implementation time of new inductors. In addition, it contributes to increasing the reliability and stability of inductor operation under harsh DC-bias conditions, ensuring high quality of the final product.

3. THEORETICAL ANALYSIS AND CALCULATION

A mathematical approach to selecting the optimal parameters of an inductor is based on the fundamental laws of electromagnetism. This method is based on Ampère's circuital law and Faraday' law of induction [48]:

$$\oint \mathbf{H} d\mathbf{l} = \sum_{\mathrm{k}} i_{\mathrm{k}} , \qquad (1)$$

which states that the circulation of the magnetic field intensity vector around a closed loop is equal to the algebraic sum of the microscopic currents enclosed by that loop;

$$E_{\mathrm{U}} = -\omega \frac{\mathrm{d}\Phi_{\mathrm{M}}}{\mathrm{d}t} = -\omega S_{\mathrm{e}} \frac{\mathrm{d}B}{\mathrm{d}t} , \qquad (2)$$

where Φ_M is the magnetic flux of induction B through surface S, S_e is the effective cross-sectional area of the magnetic core, B is the magnetic flux density (magnetic induction) in the core.

Figure 1 shows a schematic cross-sectional view of the core, demonstrating the main parameters used for the calculation.

The input data for the inductor calculation should be the following

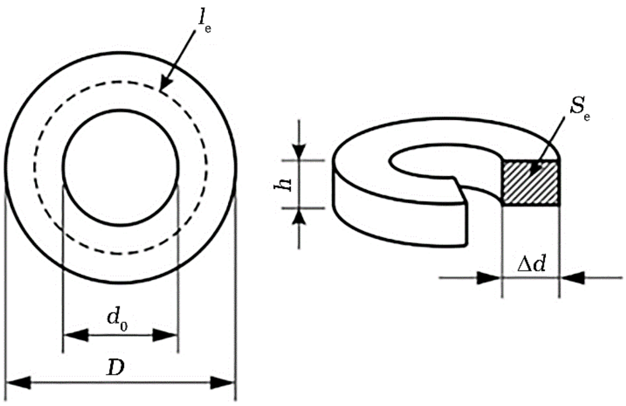

Fig. 1. Schematic cross-sectional view of the core.

parameters: I—the current, at which the inductor should operate [A], L—the required inductance of the inductor [H], J—the maximum allowable current density in the inductor winding [A/mmI], B—the maximum operating flux density (magnetic induction) of the inductor [T].

The magnetic flux density of a toroidal inductor with a ferromagnetic core is described by the following formula [49]:

$$B = \mu\mu_0 \frac{NI}{l_e}, \quad (3)$$

where μ is the relative permeability of the core, μ_0 is the permeability of vacuum, N is the number of turns of the winding, I is the current, l_e is the mean magnetic path length (effective path length) of the toroidal core.

Based on formula (3) and the fact that, for the $Fe_{73}Si_{16}B_7Cu_1Nb_3$ alloy, the saturation flux density (B_s) is limited to 1.1 T [50] (the core material enters saturation), it is important not to exceed this value to avoid core saturation. Therefore, it is necessary to select the number of turns, the mean magnetic path length, and the magnetic permeability, such that the following condition is met:

$$\mu\mu_0 \frac{NI}{l_e} \le B_S. \quad (4)$$

On the other hand, the inductance of a toroidal coil also depends on both the number of turns of the wire and the effective cross-sectional area [51]:

$$L = \frac{S_e \mu\mu_0 N^2}{l_e}. \quad (5)$$

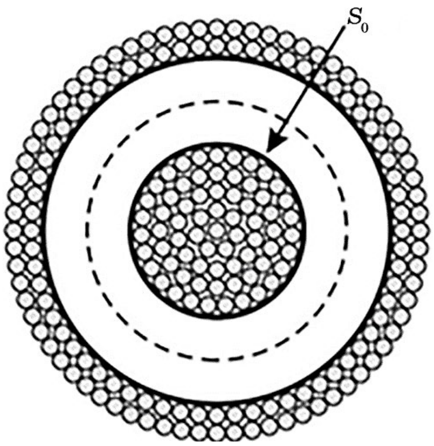

Fig. 2. Schematic cross-section showing maximum wire packing in the coil.

Another important constraint is that all the wires must fit within the core window, the area of which is S_0 (Fig. 2). The wire thickness is chosen based on the allowable current density. In most cases, it is attempted to be not exceeding a current density of 5 A/mm^2. This constraint is taken into account to ensure reliable operation of the inductive element and to prevent overheating of the wire during operation.

3.1. Core Weight Calculation Based on Permeability

The core weight can be expressed in terms of the mean path length and effective cross-sectional area as follows:

$$S_e l_e = V_e = \frac{m}{\rho} \Rightarrow m = S_e l_e \rho\,, \tag{6}$$

where S_e is effective cross-sectional area, l_e is effective path length of the core (Fig. 1), V_e is effective volume of the core, m is weight of the core [kg], ρ is density of the core material. According to Eq. (5),

$$S_e = \frac{L l_e}{\mu\mu_0 N^2}\,. \tag{7}$$

According to Eq. (3),

$$l_e = \frac{N I \mu\mu_0}{B}\,, \tag{8}$$

$$m = \frac{L}{\mu\mu_0 N^2}\frac{N I \mu\mu_0}{B}\frac{N I \mu\mu_0}{B}\rho_{\text{core}} = \frac{L I^2 \mu\mu_0}{B}\rho_{\text{core}}\,. \tag{9}$$

Therefore, based on Eq. (9), it is established that, for identical values of current and inductance, the core weight, apart from density, depends solely on the magnetic permeability of the core material. This dependence is linear, as illustrated in Fig. 3.

According to expression (9) and as seen in Fig. 3, the core weight required to manufacture an inductor with identical input requirements increases linearly with increasing core magnetic permeability. This observation allows to estimate immediately how the minimum required core weight will change, when selecting different values of core material permeability, as well as operating induction, and to account for the necessary non-magnetic gap in the core during inductor design.

This dependence can be explained as follows: with increasing magnetic permeability of the core material, it is necessary to reduce the number of wire turns to prevent material saturation. However, to ensure the required specified inductance, it is necessary to increase the cross-sectional area of the core, and therefore its weight. This can be formally expressed through the dependence of inductance on the geometrical parameters and magnetic properties of the core. When reducing the number of wire turns (N) to maintain constant inductance (L), it is necessary to increase the effective cross-sectional area (S_e) of the core. Therefore, with increasing magnetic permeability (μ), it is necessary to compensate for the decrease in the number of turns by increasing the cross-sectional area of the core. This leads to an increase in the volume (V) and, consequently, the weight (m) of the core.

This approach ensures balanced design of inductive components,

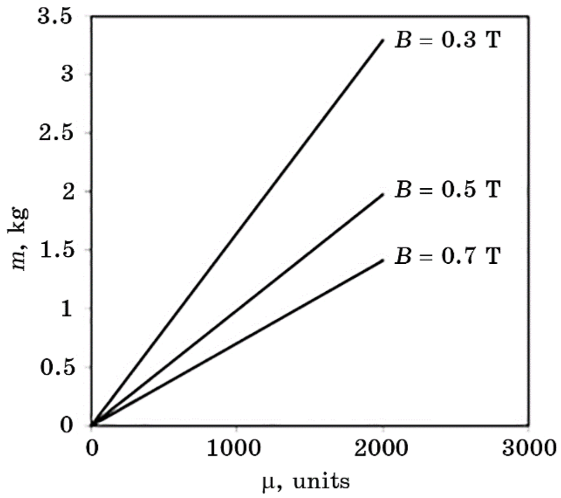

Fig. 3. Core weight *vs.* permeability of nanocrystalline $Fe_{73}Si_{16}B_7Cu_1Nb_3$ alloy for various operating inductions (for input data given in Table 1).

TABLE 1. Initial parameters for inductor design.

Parameter	Symbol	Value	Unit
Operating current	I	1	A
Target inductance	L	0.05	H
Operating magnetic flux density	B	0.7	T
Max. allowable current density	J	5	A/mm^2
Winding fill factor	K_f	0.3	–
Effective core permeability	μ_e	200	units
Core height	h	30	mm
Core material composition	–	$Fe_{73}Si_{16}B_7Cu_1Nb_3$	–
Wire material	–	Cu	–
Core price	–	200	$/kg
Wire price	–	50	$/kg

where the linear dependence of the core weight on magnetic permeability allows for precise prediction and adjustment of parameters to achieve optimal characteristics. This method is crucial for creating efficient and reliable inductors in various applications, from electronics to power systems; however, it does not consider other important parameters such as the number and thickness of wire turns, as well as whether this wire will fit within the core window (Fig. 2). This adds complexity to the design and requires additional calculations and optimization to ensure all necessary inductor characteristics.

3.2. Calculation of the Number of Wire Turns

It is necessary to find the number of turns that satisfies the following conditions, based on Eq. (4)

$$B_{max} = \mu\mu_0 \frac{NI}{l_e}$$

and Eq. (5)

$$L = \frac{S_e \mu\mu_0 N^2}{l_e},$$

in addition, considering that the wires must fit within the available core window:

$$S_e = f(N) = h \times \Delta d, \tag{10}$$

where h is core height, Δd is core thickness (Fig. 1),

$$\Delta d = \frac{l_e}{\pi} - d_0 ,$$

d_0 is core inner diameter:

$$d_0 = \sqrt{\frac{4S_0}{\pi}} .$$

To ensure that all wire turns fit within the available core window, the optimal number of turns must be calculated to satisfy these geometrical constraints. This implies that the total cross-sectional area of the wire windings must not exceed the core window area. Therefore, the sum of the cross-sectional areas of all wire turns should be less than or equal to the core window area. This can be formally expressed as follows:

$$NA_w \le S_0 = \frac{A_w N}{K_w} .$$

Then,

$$d_0 = \sqrt{\frac{4A_w N}{K_w \pi}} . \tag{11}$$

So, the final formula for the effective cross-sectional area S_e is expressed as

$$S_e = h\left(\frac{l_e}{\pi} - 2\sqrt{\frac{A_w N}{K_w \pi}}\right), \tag{12}$$

where S_0 is core window area, A_w is cross-sectional area of one wire turn, K_w is wire fill factor.

Equating expressions (12) and (7), we obtain:

$$h\left(\frac{l_e}{\pi} - 2\sqrt{\frac{A_w N}{K_w \pi}}\right) = \frac{L l_e}{\mu\mu_0 N^2} . \tag{13}$$

By performing the substitution of l_e with the value given by Eq. (8), we obtain:

$$\frac{h\mu\mu_0 NI}{B\pi} - 2h\sqrt{\frac{A_w N}{K_w \pi}} = \frac{LI}{BN} .$$

Multiplying both sides of the equation by

$$\frac{B}{Ih},$$

we obtain:

$$\frac{\mu\mu_0 N}{\pi} - \frac{2B}{I}\sqrt{\frac{A_w N}{K_w \pi}} = \frac{L}{hN}. \qquad (14)$$

Thus, we obtain the fundamental equation for the determination of the number of turns of an inductive coil, which considers inductance, operating current, the magnetic flux density of the core material, the thickness of the wire, the wire fill factor, as well as the required height of the core. For the purpose of simplification, we shall replace the input parameters with coefficients:

$$a = \frac{\mu\mu_0}{\pi},\ b = \frac{2B}{I}\sqrt{\frac{A_w}{K_w \pi}},\ c = \frac{L}{h};$$

therefore, the equation will become the final form:

$$aN - b\sqrt{N} - \frac{c}{N} = 0. \qquad (15)$$

This equation form provides a convenient way to determine the number of turns using the given coefficients a, b, and c, which take into account the physical and geometrical parameters of the core and its operating regimes.

3.3. Effect of DC Bias on Magnetic Permeability

The magnetic permeability of a core material is one of the key parameters determining its ability to conduct effectively a magnetic field. However, magnetic permeability is not a constant value and can vary under the influence of a DC-bias current. This dependence is crucial for the design of inductive components, such as chokes and transformers, which operate under DC-bias conditions.

As the DC-bias current increases, the magnetic permeability of the core material typically goes through several stages. At initial bias levels, the magnetic permeability may remain relatively stable. This is explained by the fact that the magnetic domains within the core material are easily oriented along the applied magnetic field, which maintains high magnetic permeability.

However, as the DC-bias current increases to a certain critical level, the magnetic permeability begins to decrease. This process is known as core saturation. In the saturation stage, most magnetic domains are already oriented, and further increases in current do not lead to a significant increase in magnetic flux density. Instead, the magnetic permeability begins to decrease gradually, and with further increases in the DC current, a gradual drop in permeability occurs.

This nonlinear dependence is of significant importance for the design of inductive components. For example, in soft magnetic composite (SMC) cores, this dependence determines the operating characteristics of the components at various DC-bias current levels. Taking this dependence into account allows engineers to predict accurately the change in inductance and the performance of the components under various operating conditions.

The dependence of magnetic permeability on DC-bias current is determined experimentally for each individual core material. This dependence is unique to each material type and strongly depends on its physical properties, as well as the value of the effective magnetic permeability. Due to the complexity and variability of the physical processes occurring in the core material under the influence of DC-bias current, modelling this dependence is a rather complex task.

In our formula, we do not include the effect of DC-bias current. Instead, we use experimental data showing how the effective magnetic permeability changes with DC bias, since accurately predicting this is hard and not part of this work.

As an illustration, the relationship between magnetic permeability and DC-bias current for the $Fe_{73}Si_{16}B_7Cu_1Nb_3$ alloy is depicted in Fig. 4 with curves shown for effective permeabilities of 30 and 60 units.

The graph demonstrates the change in magnetic permeability with increasing DC-bias current, illustrating characteristic stages: initial stability, gradual decrease, and a sharp drop in permeability. The pre-

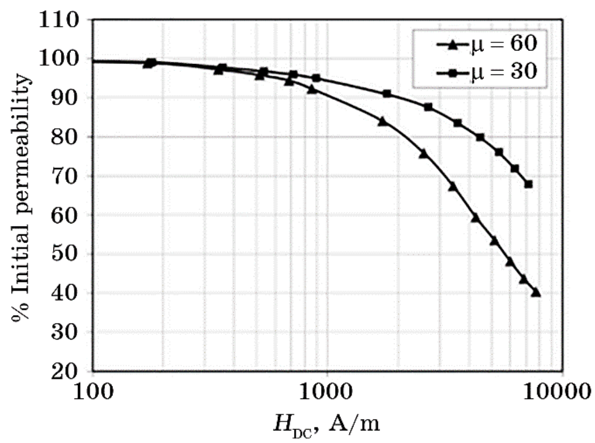

Fig. 4. Effective permeability as a function of DC bias current for the nanocrystalline $Fe_{73}Si_{16}B_7Cu_1Nb_3$ core with an air gap.

sented data are crucial for understanding the materials' behaviour under real operating conditions and are used for accurate modelling and optimization of inductive components.

3.4. Application of the Proposed Inductor Calculation Approach for Nanocrystalline $Fe_{73}Si_{16}B_7Cu_1Nb_3$ Cores: a Worked Example

The formula (15) we derived for calculating the number of turns is a non-linear equation of the form

$$ax - b\sqrt{x} - \frac{c}{x} = 0\,.$$

However, this equation does not always yield a result. To obtain a result, the function

$$f(x) = ax - b\sqrt{x} - \frac{c}{x} \tag{16}$$

must intersect the x-axis at least once. This depends on the specific values of the constants a, b, and c. Graphical analysis of the function can reveal the presence or absence of such intersection points. If the curve does not intersect the x-axis, then, the equation has no solutions.

The x-intercept of the graph of the function defined by Eq. (16) corresponds to a root of Eq. (15). The term c/x in both equations becomes undefined at $x = 0$. Furthermore, due to the presence of $\sqrt{x}$, the domain of both equations is restricted to $x > 0$. Given the complexity of analytical solutions, the graphical method is a valuable tool for visualizing the behaviour of the function $f(x)$ in the domain $x > 0$ and for approximating its real roots.

Based on the foregoing, we will consider an example of determining the number of turns of an inductor using a graphical method, utilizing the input data presented in Table 1.

The cross-sectional area of the wire is calculated based on the maximum allowable current density J:

$$A_{\mathrm{w}} = \frac{I}{J} = \frac{1}{5} = 0.2\ [\mathrm{mm}^2].$$

As we know, the equation for determining the number of turns of the inductor takes the form (15), where a, b, and c are constants that depend on the inductor-design parameters (including the inductance L, magnetic flux density B, effective core permeability μ_e, and core geometry).

To solve this equation, we will use the graphical method. This method involves plotting the function (16), where x represents the number of turns (N) of the inductor coil. The points, where the graph intersects the x-axis (where $f(x) = 0$), correspond to the solutions of the equation, *i.e.*, the values of N, for which the equality holds. The graphical representation for the given parameters, with the number of turns (N) plotted on the x-axis and the values of the function $f(x)$ on the y-axis, is shown in Fig. 5.

The graph illustrates the relationship between the function $f(N)$ and the number of turns (N) for a toroidal inductor. The x-axis represents N on a logarithmic scale ($\log_{10}$), and the y-axis represents the value of $f(N)$.

The graph demonstrates that, at a small number of turns, $f(N)$ decreases sharply (becomes more negative), indicating a significant influence of N on the equation result, which is indirectly related to inductance. As N increases, $f(N)$ gradually increases (becomes less negative) and asymptotically approaches zero, indicating a diminishing influence of further increases in N.

Three distinct regions can be observed:

sharp decrease from 1 to approximately 10 turns, when $f(N)$ shows a steep drop (increase in absolute value);

gradual increase from 10 to 100 turns, when $f(N)$ continues to increase (approaching zero), but more gradually;

approaching zero with more than 100 turns, when $f(N)$ almost stabilizes asymptotically approaching zero.

This curve shape allows determining the optimal number of turns to achieve the desired electrical characteristics. In this case, the optimal number of turns corresponds to the point, where the graph most closely approaches the x-axis (where $f(N) \cong 0$), which represents a solution of

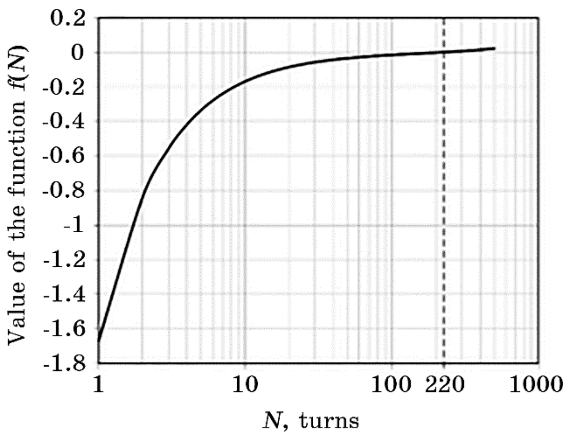

Fig. 5. Graphical solution of Eq. (16) for determining the number of turns of a toroidal inductor with the $Fe_{73}Si_{16}B_7Cu_1Nb_3$ core (based on input data presented in Table 1).

the equation for the given parameters. The graph does not intersect the x-axis, but $f(N)$ is closest to zero at $N \cong 220$ (Fig. 5).

Knowing the number of turns, the cores' physical dimensions can now be calculated, taking into account the relevant parameters and its geometry. The following calculations determine the inner, mean, and outer diameters, as well as the mean path length of the core. The inner diameter is determined based on the required winding area within the core window, using Eq. (11), assuming all wire turns fit within this space:

$$d_0 = \sqrt{\frac{4A_\mathrm{w}N}{K_\mathrm{w}\pi}} = 13.51 \text{ [mm]}.$$

The mean path length of the core, according to Eq. (8), is determined as

$$l_\mathrm{e} = \frac{NI\mu\mu_0}{B} = 77.19 \text{ [mm]}.$$

Radial thickness of the core (see Fig. 1) is

$$\Delta d = \frac{l_\mathrm{e}}{\pi} - d_0 = 11.06 \text{ [mm]}.$$

The core outer diameter can now be calculated using the following expression, given its inner diameter and radial thickness:

$$D = d_0 + 2\Delta d = 35.63 \text{ [mm]}.$$

3.5. Calculation of Electrical Power Losses

In inductors operating under DC-bias conditions, various types of losses exist. The main ones are winding losses, hysteresis losses, and eddy current losses [51].

Total losses (P_total) can be expressed as the sum of different types of losses:

$$P_\mathrm{total} = P_\mathrm{h} + P_\mathrm{e} + P_\mathrm{exc},$$

where P_h represents hysteresis losses, P_e represents eddy current losses, and P_exc represents excess losses. The nature of excess losses is not yet fully understood; these losses depend on mechanical stresses within the material and resonance losses. They become significant at very low induction levels and very high frequencies; therefore, these losses are usually ignored. Other types of losses, such as winding losses or losses related to other mechanisms affecting the efficiency of magnetic devices, can also be included.

Hysteresis and eddy current losses can be significant in some cases, but for inductors operating under DC-bias conditions, their magnitude is usually small (except when the core operates near saturation).

Hysteresis losses are caused by the remagnetisation of the core and depend on the area of the hysteresis loop. Furthermore, these losses are linearly dependent on frequency, since an increase in frequency leads to a greater number of remagnetisation cycles per unit of time, which results in an increase in total hysteresis losses.

Hysteresis losses can be described by the following empirical relationship:

$$P_h = K_h B_m^x f ,$$

where K_h and x are parameters, which depend on the material and its structural aspects, B_m is the peak magnetic flux density, and f is the frequency [29].

Eddy currents, in turn, are induced in the conductive core material by the alternating magnetic field and have a non-linear dependence on the frequency and amplitude of this field [29–32]. The empirical value of such losses can be expressed as

$$P_e = \frac{(\pi d_e B_m)^2 f}{\beta \rho_b R_b},$$

where d_e is the effective diameter of the ferromagnetic material particles, ρ_b is the density of these material particles, R_b is the specific electrical resistivity, and β is a geometrical coefficient [32].

To reduce eddy current losses, cores are typically made of thin insulated laminations or materials with high specific resistivity.

It is important to note that both eddy current and hysteresis losses are significantly reduced when operating at low frequencies, which is characteristic of DC-bias conditions. However, as the frequency increases, hysteresis losses can become more significant, even with small eddy current magnitudes.

Therefore, the losses in an inductor operating under DC-bias conditions primarily consist of winding losses, which are most often due to the copper wire. All other types of losses are of negligible magnitude and can therefore be neglected in this analysis (if the core is not operating near saturation).

The winding losses of the inductor are caused by the ohmic resistance of the copper wire. To calculate these losses, it is necessary to know the resistivity of copper ($\rho_{Cu} = 0.017 \cdot 10^{-6}$ Ohm·m) and the geometrical parameters of the winding. The resistance of the copper wire can be calculated based on its length and cross-sectional area:

$$l_w = pN\,,$$

where p is the perimeter of the cross-section of the toroidal core, and

$$p = D - d_0 + 2h\,.$$

The resistance of a wire is calculated using the following formula:

$$R_w = \rho\frac{l_w}{A_w} = \rho N\frac{(D - d_0 + 2h)}{A_w} = 0.96\ \text{[Ohm]}.$$

Copper wire losses are determined by the formula

$$P_w = I^2 R_w = 0.96\ \text{[W]}.$$

In inductors operating under DC-bias conditions, the main losses occur in the winding and are largely determined by its ohmic resistance. These losses, referred to as winding losses (or I^2R losses), can be calculated based on the resistivity of copper and the geometrical parameters of the winding, including the length and cross-sectional area of the wire. Hysteresis and eddy-current losses in the core are also present, but winding losses are often dominant, especially at low frequencies. Other types of losses, such as radiation losses, are usually negligible and can be ignored in the analysis (unless the core is operating near saturation).

3.6. Cost-Based Optimization of Inductor Design

The cost of an inductor is a key factor in its design. According to the methodology described above, the inductor cost depends on a set of interrelated parameters, among which the key ones are the relative permeability of the core material (μ_r), the core height (h), and the number of turns (N). These parameters are interconnected and affect the core dimensions (inner and outer diameters, mean length of the magnetic path), the amount of wire required, and therefore the overall cost of the product. Therefore, it is important to find the optimal balance between μ_r, h, and N, which ensures minimum cost for given requirements for weight, losses, and manufacturability. It is known that

$$h = \frac{D - d_0}{2}$$

ensures the minimum wire length, and

$$h = \frac{2}{3}\frac{D - d_0}{2}$$

ensures better manufacturability and a smaller inductor area.

To analyse the inductor parameters, Table 2 was constructed, in which the number of turns required to achieve a given inductance was calculated for each value of the core-materials' relative permeability and core height from the specified range. The input data for the calculations, such as the inductor geometrical dimensions (inner and outer diameters), inductance, wire and core material, and their cost, are presented in Table 1.

To determine the optimal inductor parameters for a given inductance, the cost of the finished product was calculated for each combination of relative permeability, core height, and number of turns in Table 2. To represent visually the results, a gray-scale gradient was used to illustrate the cost dependence on these parameters. (Specifically, white (unfilled) cells correspond to a price exceeding 120% of the minimum cost, light grey shading indicates a price in the range of 110–120% of the minimum cost, dark grey shading corresponds to a price up to 110% of the minimum cost, black shading represents the minimum inductor cost.)

Thus, by varying the core height, it is possible to construct a table that clearly shows the cost of the finished product depending on the relative permeability, core height, and number of turns. Analysis of the obtained data allows selecting a combination of these parameters that ensures the minimum cost of the finished product. This approach, by balancing manufacturability, cost, weight, or other necessary characteristics, enables the determination of optimal parameters for inductor manufacturing under specific conditions.

TABLE 2. Inductor turns as a function of relative permeability and core height.

$\mu\backslash h$, mm	5	10	20	30	40	50	100
19	7600	7400	7300	7300	7300	7300	7300
26	4300	4100	4000	4000	4000	3900	3900
40	2200	2000	1800	1800	1800	1700	1700
60	1300	1100	940	880	850	830	780
90	850	680	550	500	460	440	390
125	640	490	390	340	310	290	250
147	570	430	330	290	260	250	200
160	530	400	310	270	240	230	180
175	500	380	290	250	220	210	170
200	450	340	260	220	200	180	150

3.7. Software Algorithm for Inductor Parameter Calculation

For ease of practical application, a program has been developed, the algorithm of which can be represented by the following flowchart (Fig. 6).

The program contains three nested loops that provide a sequential iteration through all variable parameters included in the calculation. At the highest level, the loop iterates through all values of the relative permeability array (μ), for example, 14, 19, 26, 40, 60, *etc*. At the middle level, the values of the core height (h) are iterated, which are also taken from a data array (for example, 5, 10, 15, 20 mm). At the lowest level, all possible values of the number of turns (N) are iterated (from $N = 1$ to the maximum specified value N_{max}), and the main condition is checked—the toroidal core window area (S_0) must be greater than or equal to the wire cross-sectional area (A_w) (taking into account the fill factor).

The automated calculation begins with the input of initial data, where the initial values of relative permeability (μ), core height (h), and number of turns (N) are set. The loop condition check starts with verifying whether the current value of μ exceeds the maximum allowable value from the specified range (μ_{max}). If the condition is met, the

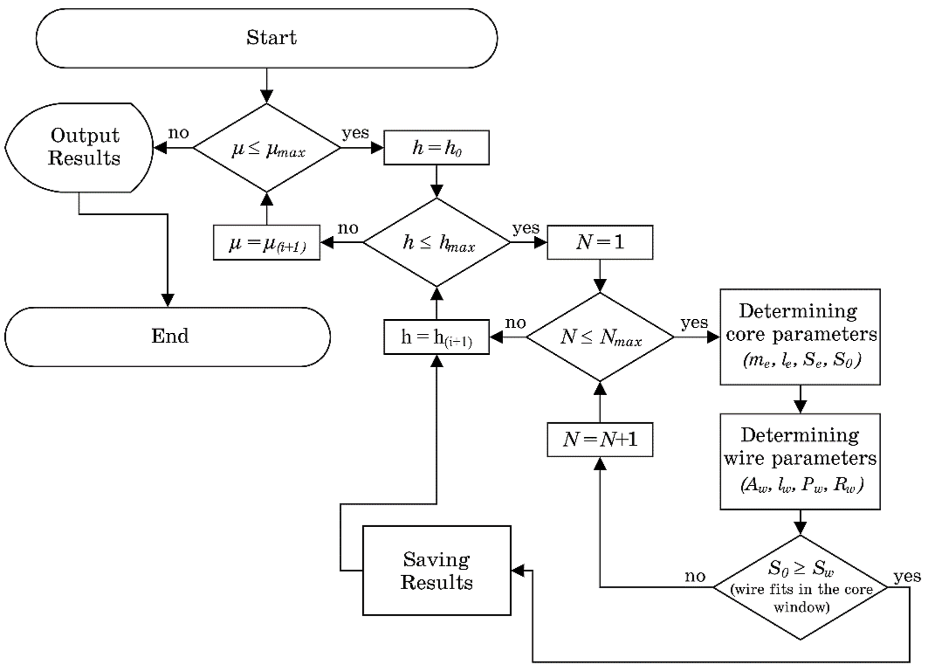

Fig. 6. Algorithm flowchart for inductor design.

loop proceeds to the next value of μ. Similarly, the condition for the core height (h) is checked, and if the current value does not exceed the maximum allowable value from the specified range (h_{max}), the loop proceeds to the next value of h. Next, the condition for the number of turns (N) is checked, and if the current value does not exceed the maximum allowable value from the specified range (N_{max}), the loop proceeds to the next value of N.

After the condition checks are performed, the program proceeds to calculate the core parameters, such as the effective volume (V_e), mean path length (l_e), effective cross-sectional area (S_e), core weight (m_e), and others. Then, the wire parameters are calculated, such as the cross-sectional area (A_w), length (l_w), resistance (R_w), and winding losses (P_w). The main condition is checked by comparing the toroidal core window area (S_0) with the wire cross-sectional area (S_w). If the condition $S_0 \geq A_w$ is met (*i.e.*, the wire fits within the core window considering the fill factor), the calculated parameters are stored, and the program proceeds to the next iteration of the core height loop (h).

This approach significantly reduces the development and implementation time of new inductors due to calculation automation, ensuring high accuracy and compliance with technical requirements. The automated calculation program takes into account all key parameters affecting the inductor operation and allows determining the optimal values of relative permeability, core height, and number of turns to achieve the best results in terms of weight, losses, and product cost. The use of such a program contributes to increased design efficiency, optimization of material usage, and reduction of inductive component manufacturing costs. In addition, the proposed program allows rapid adaptation of calculations to various technical requirements and parameters, which is important in today's rapidly developing technologies.

4. CONCLUSIONS

A novel methodology, based on a developed analytical formula, has been created for calculating the parameters of linear chokes based on specified operational requirements. This methodology enables the calculation of the dimensions, weight, losses, and cost of both the nanocrystalline $Fe_{73}Si_{16}B_7Cu_1Nb_3$ core, considering its unique properties under DC bias conditions, and the resulting linear choke. Examples of tabular and graphical representations of the calculation results are provided, facilitating the selection of an optimal choke design based on cost and/or dimensions.

The universality and novelty of the proposed method lie in its applicability to the calculation of toroidal cores made of not only of nanocrystalline $Fe_{73}Si_{16}B_7Cu_1Nb_3$ alloy, but also of any other alloys and their composites, such as tape-wound or powder cores based on iron, Sendust, permalloy, or ferrites. This allows for unified calculations based on the required operating characteristics of the choke, independent of the product catalogues of various manufacturers. This adaptability makes the methodology highly valuable for a wide range of applications and simplifies the design process by providing a single, comprehensive calculation framework.

A promising area for the application of the developed methodology is the automotive, aviation, and aerospace industries, where the weight and dimensions of dozens of inductive components play a crucial role. The high efficiency, reliability, and weight reduction achieved by using nanocrystalline toroidal cores made of $Fe_{73}Si_{16}B_7Cu_1Nb_3$ alloy make this material highly attractive for use in these high-tech sectors. The ability to optimize choke design using the proposed methodology directly contributes to improving the performance and efficiency of systems in these demanding applications.

In addition to the analytical calculations, a software implementation of the proposed methodology has been developed. This software tool automates the design process, allowing for rapid and accurate calculation of choke parameters based on user-defined inputs. This automation significantly reduces design time and the potential for human error.

REFERENCES

1. X. Zheng, T. Ishimine, S. Yamamoto, T. Tokuoka, S. Ohashi, K. Matsunuma, H. Fujikawa, and T. Hayasaki, *SEI Technical Review*, **75**: 55 (2012).
2. H. S. Silvus and R. E. White, *SAE Transactions*, **111**: 37 (2002).
3. C. Sullivan and A. Muetze, *IEEE Trans. Ind. Appl.*, **46**, Iss. 2: 884 (2010).
4. O. Coşkun, R. Eken, Ö. Çevik, and G. Yılmaz, *Analog Integr. Circ. Sig. Process.*, **113**: 197 (2022).
5. V. Gurevich, *Electr. Eng. Electromech.*, **2**: 71 (2016).
6. M. Thian, V. Fusco, and P. Gardner, *IEEE TCAS-I*, **58**, No. 3: 451 (2011).
7. H. W. Ott, *Electromagnetic Compatibility Engineering (Rev. Ed.)* (Hoboken, New Jersey: John Wiley & Sons, Inc.: 2009).
8. A. M. Bamdas and Yu. A. Savinovskiy, *Drosseli Fil'trov Radioapparatury* [Chokes of Radio Equipment Filters] (Moskva: Sovetskoye Radio: 1962) (in Russian).
9. V. S. Rudenko, V. Ya. Romashko, and V. V. Tryfoniuk, *Promyslova Ehlektronika: Pidruchnyk* [Industrial Electronics: Textbook] (Kyiv: Lybid': 1993) (in Ukrainian).
10. B. S. Baitalyuk, V. A. Maslyuk, S. B. Kotlyar, and Ya. A. Sytnyk, *Powder Metall. Met. Ceram.*, **55**: 496 (2016).
11. Z. Zheng, S. Li, and K. Peng, *J. Magn. Magn. Mater.*, **568**: 170423 (2023).
12. G. E. Fish, *Proc. IEEE*, **78**, No. 6: 947 (1990).
13. J. L. Ni, F. Duan, S. J. Feng, F. Hu, X. C. Kan, and X. S. Liu, *J. Alloys Compd.*,

897: 163191 (2022).
14. B. D. Cullity and C. D. Graham, *Introduction to Magnetic Materials. Second Edition* (Hoboken, New Jersey: John Wiley & Sons, Inc.: 2009).
15. F. Fiorillo, *Characterization and Measurement of Magnetic Materials. 1st Edition* (Eds. I. D. Mayergoyz) (Academic Press: 2004).
16. Z. Y. Wu, Z. Jiang, X. A. Fan, L. J. Zhou, W. L. Wang, and K. Xu, *J. Alloys Compd.*, **742**: 90 (2018).
17. G. Ouyang, X. Chen, Y. Liang, C. Macziewski, and J. Cui, *J. Magn. Magn. Mater.*, **481**: 234 (2019).
18. W. Li, Y. Zheng, Y. Kang, A. Masood, Y. Ying, J. Yu, J. Zheng, L. Qiao, J. Li, and S. Che, *J. Alloys Compd.*, **819**: 153028 (2020).
19. D. Azuma, N. Ito, and M. Ohta, *J. Magn. Magn. Mater.*, **501**: 166373 (2019).
20. R. Hasegawa, *J. Magn. Magn. Mater.*, **324**, No. 21: 3555 (2012).
21. S. Lu, M. Wang, and Z. Zhao, *J. Non-Cryst. Solids*, **616**: 122440 (2023).
22. X. Wang, Z. Lu, C. Lu, G. Li, and D. Li, *J. Iron Steel Res. Int.*, **21**, No. 11: 1055 (2014).
23. C. Chang, J. Guo, Q. Li, S. Zhou, M. Liu, and Y. Dong, *J. Alloys Compd.*, **788**: 1177 (2019).
24. R. Ma and P. Yu, *Mater. Res. Bull.*, **139**: 111256 (2021).
25. H. Shokrollahi and K. Janghorban, *J. Mater. Process. Technol.*, **189**, Nos. 1–3: 1 (2007).
26. K. L. Alvarez, H. A. Baghbaderani, J. M. Martín, N. Burgos, M. Ipatov, Z. Pavlovic, and J. Gonzalez, *J. Magn. Magn. Mater.*, **501**: 166457 (2020).
27. Y. Yoshizawa, S. Fujii, D. H. Ping, M. Ohnuma, and K. Hono, *Scr. Mater.*, **48**, No. 7: 863 (2003).
28. A. Krings, A. Boglietti, A. Cavagnino, and S. Sprague, *IEEE Trans. Ind. Electron.*, **64**, No. 3: 2405 (2017).
29. P. Kollár, Z. Birčáková, J. Füzer, R. Bureš, and M. Fáberová, *J. Magn. Magn. Mater.*, **327**: 146 (2013).
30. L. O. Hultman and A. G. Jack, *Proc. of IEEE International Electric Machines and Drives Conference, 2003. IEMDC'03. (Madison, WI, USA: 2003)*, vol. **1**, p. 516.
31. M. Polak, J. Kvitkovic, P. Mozola, E. Usak, P. N. Barnes, and G. A. Levin, *Supercond. Sci. Technol.*, **20**, No. 9: 293 (2007).
32. M. Lauda, J. Füzer, P. Kollár, M. Strečková, R. Bureš, J. Kováč, M. Baťková, and I. Baťko, *J. Magn. Magn. Mater.*, **411**: 12 (2016).
33. *Handbook of Magnetic Materials* (Eds. K. H. J. Buschow). *Elsevier Science B.V. Vol.* ***10*** (Netherlands: North-Holland: 1997).
34. V. K. Nosenko, *Visnyk Natsionalnoi Akademii Nauk Ukrainy*, **4**: 68 (2015) (in Ukrainian).
35. V. V. Maslov, V. K. Nosenko, L. E. Taranenko, and A. P. Brovko, *Fiz. Met. Metalloved.*, **91**, No. 5: 47 (2001).
36. A.-L. Adenot-Engelvin, C. Dudek, F. Bertin, and O. Acher, *J. Magn. Magn. Mater.*, **316**: e831 (2007).
37. M. Manivel Raja, K. Chattopadhyay, B. Majumdar, and A. Narayanasamy, *J. Alloys Compd.*, **297**: 199 (2000).
38. J. A. Moya, *J. Alloys Compd.*, **622**: 635 (2015).
39. N. Shen, Z. Dou, Y. Li, K. Lv, Y. Wu, F. Li, and X. Hui, *Mater. Lett.*, **305**: 130759 (2021).

40. K. Takenaka, A. D. Setyawan, Y. Zhang, P. Sharma, N. Nishiyama, and A. Makino, *Mater. Trans.*, **56**, Iss. 3: 372 (2015).
41. I. I. Leopol'skiy and L. G. Pikalova, *Raschyot Transformatorov i Drosseley Maloy Moshchnosti* [Calculation of Low-Power Transformers and Chokes] (Moskva– Leningrad: Gosehnergoizdat: 1963) (in Russian).
42. I. N. Sidorov, V. V. Ukoseyev, and A. A. Khristinin, *Malogabaritnyye Transformatory i Drosseli: Spravochnik* [Small-Sized Transformers and Chokes: Handbook] (Moskva: Radio i Svyaz': 1985) (in Russian).
43. *Istochniki Ehlektropitaniya Radioehlektronnoy Apparatury: Spravochnik* [Power Sources of Radioelectronic Equipment: Handbook] (Ed. G. S. Nayvelt) (Moskva: Radio i Svyaz': 1986) (in Russian).
44. K. B. Mazel', *Vypryamiteli i Stabilizatory Napryazheniya* [Rectifiers and Voltage Stabilizers] (Moskva–Leningrad: Gosehnergoizdat: 1951) (in Russian).
45. A. Ayachit, D. K. Saini, M. K. Kazimierczuk, and A. Reatti, *Proc. of IECON 2016—42nd Annual Conference of the IEEE Industrial Electronics Society (Florence, Italy: 2016)*, p. 5621–5626.
46. Wm. T. McLyman, *Transformer and Inductor Design Handbook (4th Ed.)* (Boca Raton, FL, USA: CRC Press: 2011).
47. A. E. Da Silva Bento, *Toroid Inductor Development for a SIC DC–DC Converter up to 150 kW, Based on Finite Element Method* (Lisboa: Instituto Superior De Engenharia De Lisboa: 2015).
48. L. D. Didukh, *Ehlektryka ta Magnetyzm: Pidruchnyk* [Electricity and Magnetism: Textbook] (Ternopil: Pidruchnyky i Posibnyky: 2020) (in Ukrainian).
49. F. Cardarelli, *Magnetic Materials. Materials Handbook* (Cham: Springer: 2018).
50. A. Nosenko, T. Mika, O. Rudenko, Y. Yarmoshchuk, and V. Nosenko, *Nanoscale Res. Lett.*, **10**: 136 (2015).
51. W. G. Hurley and W. H. Wölfle, *Transformers and Inductors for Power Electronics: Theory, Design and Applications* (John Wiley & Sons Ltd: 2013).